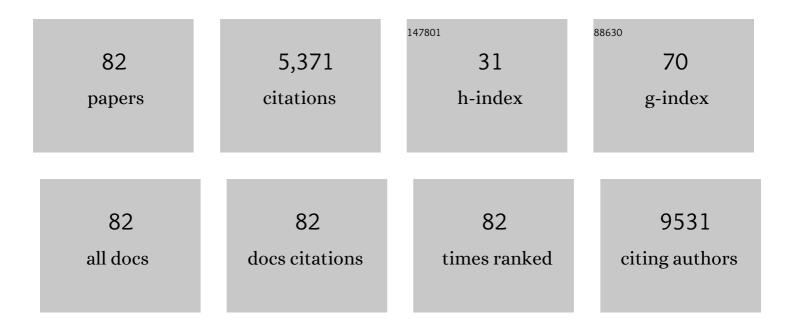


List of Publications by Year in descending order

Source: https://exaly.com/author-pdf/9415147/publications.pdf Version: 2024-02-01



K VI HE

#	Article	IF	CITATIONS
1	In situ transmission electron microscopy and artificial intelligence enabled data analytics for energy materials. Journal of Energy Chemistry, 2022, 68, 454-493.	12.9	33
2	van der Waals Semiconductor Empowered Vertical Color Sensor. ACS Nano, 2022, 16, 8619-8629.	14.6	5
3	Cryogenic electron microscopy for emerging materials research: From quantum materials to energy applications. MRS Communications, 2022, 12, 471-482.	1.8	1
4	In Situ TEM Study on Conversionâ€īype Electrodes for Rechargeable Ion Batteries. Advanced Materials, 2021, 33, e2000699.	21.0	58
5	TEM Characterization of Battery Materials. , 2021, , .		1
6	Tuning MOF-Derived Co ₃ O ₄ /NiCo ₂ O ₄ Nanostructures for High-Performance Energy Storage. ACS Applied Energy Materials, 2021, 4, 1537-1547.	5.1	46
7	Single Atomic Iron Site Catalysts via Benign Aqueous Synthesis for Durability Improvement in Proton Exchange Membrane Fuel Cells. Journal of the Electrochemical Society, 2021, 168, 044501.	2.9	10
8	Origin of anomalous high-rate Na-ion electrochemistry in layered bismuth telluride anodes. Matter, 2021, 4, 1335-1351.	10.0	26
9	Identification of Topological Spin Textures in Frustrated Fe3Sn2 Magnetic System. Microscopy and Microanalysis, 2021, 27, 928-929.	0.4	0
10	Temperature-Dependent Structural Evolution of Pt-Ni Nanoparticles Observed by In Situ TEM. Microscopy and Microanalysis, 2021, 27, 1236-1237.	0.4	0
11	Resolving Grain Boundary Microstructures in Garnet-Type Li7La3Zr2O12 using Model-Based TEM Image Simulation. Microscopy and Microanalysis, 2021, 27, 1758-1759.	0.4	0
12	Probing Microstructure-Dependent Ionic Conductivity and Stability of Garnet Solid Electrolytes through In Situ TEM with Operando Impedance Spectroscopy. Microscopy and Microanalysis, 2021, 27, 1506-1507.	0.4	1
13	A high-entropy phosphate catalyst for oxygen evolution reaction. Nano Energy, 2021, 86, 106029.	16.0	100
14	Novel twin-perovskite nanocomposite of Ba–Ce–Fe–Co–O as a promising triple conducting cathode material for protonic ceramic fuel cells. Journal of Power Sources, 2020, 450, 227609.	7.8	52
15	Enhancing nanostructured nickel-rich lithium-ion battery cathodes via surface stabilization. Journal of Vacuum Science and Technology A: Vacuum, Surfaces and Films, 2020, 38, 063210.	2.1	8
16	High Volumetric Energy and Power Density Li2TiSiO5 Battery Anodes via Graphene Functionalization. Matter, 2020, 3, 522-533.	10.0	27
17	Grain-boundary structure and segregation in Nb3Sn coatings on Nb for high-performance superconducting radiofrequency cavity applications. Acta Materialia, 2020, 188, 155-165.	7.9	24
18	A New Cryo-FIB-TEM Approach for Damage-free Characterization of Garnet Electrolytes in Solid-state Batteries. Microscopy and Microanalysis, 2020, 26, 2784-2785.	0.4	5

ΚΑΙ ΗΕ

#	Article	lF	CITATIONS
19	Red-phosphorus-impregnated carbon nanofibers for sodium-ion batteries and liquefaction of red phosphorus. Nature Communications, 2020, 11, 2520.	12.8	77
20	Air-protective Cryo-FIB Tomography of Sensitive Materials for Energy Applications. Microscopy and Microanalysis, 2020, 26, 1828-1829.	0.4	7
21	Orientationâ€Dependent Intercalation Channels for Lithium and Sodium in Black Phosphorus. Advanced Materials, 2019, 31, e1904623.	21.0	44
22	In Situ Electron Microscopy for Electrically Induced Charge Transport and Phase Transformation. Microscopy and Microanalysis, 2019, 25, 1862-1863.	0.4	0
23	Role of surface reconstruction on Cu/TiO2 nanotubes for CO2 conversion. Applied Catalysis B: Environmental, 2019, 255, 117754.	20.2	32
24	Atomic-scale analyses of Nb ₃ Sn on Nb prepared by vapor diffusion for superconducting radiofrequency cavity applications: a correlative study. Superconductor Science and Technology, 2019, 32, 024001.	3.5	25
25	Rational anode design for protonic ceramic fuel cells by a one-step phase inversion method. Journal of Power Sources, 2019, 418, 162-166.	7.8	18
26	Enhanced visible-light photoelectrochemical hydrogen evolution through degradation of methyl orange in a cell based on coral-like Pt-deposited TiO2 thin film with sub-2 nm pores. Catalysis Today, 2019, 335, 333-344.	4.4	30
27	Multistep Lithiation of Tin Sulfide: An Investigation Using <i>in Situ</i> Electron Microscopy. ACS Nano, 2018, 12, 3638-3645.	14.6	50
28	Panoramic Visualization of Lithiation of Copper Sulfide by In Situ STEM. Microscopy and Microanalysis, 2018, 24, 1498-1499.	0.4	1
29	Thin Film RuO ₂ Lithiation: Fast Lithiumâ€ l on Diffusion along the Interface. Advanced Functional Materials, 2018, 28, 1805723.	14.9	11
30	Mechanistic Origin of the High Performance of Yolk@Shell Bi ₂ S ₃ @N-Doped Carbon Nanowire Electrodes. ACS Nano, 2018, 12, 12597-12611.	14.6	213
31	Lithium-Ion Batteries: Atomic-Scale Observation of Electrochemically Reversible Phase Transformations in SnSe2 Single Crystals (Adv. Mater. 51/2018). Advanced Materials, 2018, 30, 1870393.	21.0	4
32	In-situ Investigation of Multi-Step Lithiation of Tin Sulfide. Microscopy and Microanalysis, 2018, 24, 1864-1865.	0.4	0
33	Atomicâ€Scale Observation of Electrochemically Reversible Phase Transformations in SnSe ₂ Single Crystals. Advanced Materials, 2018, 30, e1804925.	21.0	38
34	<i>In Situ</i> Observation of Resistive Switching in an Asymmetric Graphene Oxide Bilayer Structure. ACS Nano, 2018, 12, 7335-7342.	14.6	36
35	In Situ Atomic-Scale TEM Observation of Phase Transformation in Two-Dimensional SnSe2 Single Crystals. Microscopy and Microanalysis, 2018, 24, 1862-1863.	0.4	1
36	Visualizing the toughening origins of gel-grown calcite single-crystal composites. Chinese Chemical Letters, 2018, 29, 1666-1670.	9.0	12

ΚΑΙ ΗΕ

#	Article	IF	CITATIONS
37	Ultrafast light-induced symmetry changes in single BaTiO ₃ nanowires. Journal of Materials Chemistry C, 2017, 5, 1522-1528.	5.5	16
38	Ag–Sn Bimetallic Catalyst with a Core–Shell Structure for CO ₂ Reduction. Journal of the American Chemical Society, 2017, 139, 1885-1893.	13.7	455
39	In Situ Synthesis of Highly Dispersed and Ultrafine Metal Nanoparticles from Chalcogels. Journal of the American Chemical Society, 2017, 139, 2900-2903.	13.7	68
40	Kinetically-Driven Phase Transformation during Lithiation in Copper Sulfide Nanoflakes. Nano Letters, 2017, 17, 5726-5733.	9.1	67
41	In Situ Observation of Structural Change in Single-Crystalline LiFePO4 Nanoflakes during Electrochemical Cycling. Microscopy and Microanalysis, 2017, 23, 1988-1989.	0.4	2
42	Towards Understanding Ionic Transport Mechanisms of Sodium in Graphitic Materials by In Situ TEM. Microscopy and Microanalysis, 2017, 23, 1974-1975.	0.4	0
43	Rapid alignment of nanotomography data using joint iterative reconstruction and reprojection. Scientific Reports, 2017, 7, 11818.	3.3	75
44	Direct Visualization of Lithium Intercalation in Spinel Iron Oxide by In-Situ Bright-Field Scanning Transmission Electron Microscopy. Microscopy and Microanalysis, 2016, 22, 760-761.	0.4	1
45	Visualizing non-equilibrium lithiation of spinel oxide via in situ transmission electron microscopy. Nature Communications, 2016, 7, 11441.	12.8	162
46	In Situ STEM-EELS Observation of Nanoscale Interfacial Phenomena in All-Solid-State Batteries. Nano Letters, 2016, 16, 3760-3767.	9.1	278
47	Radiation-induced solidification of ionic liquid under extreme electric field. Nanotechnology, 2016, 27, 375701.	2.6	16
48	Kinetic Phase Evolution of Spinel Cobalt Oxide during Lithiation. ACS Nano, 2016, 10, 9577-9585.	14.6	54
49	Interaction of Black Phosphorus with Oxygen and Water. Chemistry of Materials, 2016, 28, 8330-8339.	6.7	436
50	Comparison of Co3O4 and CoO Nanoparticles as Anodes for Lithium-ion Batteries. Microscopy and Microanalysis, 2015, 21, 477-478.	0.4	2
51	Contrasting Reaction Modality between Electrochemical Sodiation and Lithiation in NiO Conversion Electrode Materials. Microscopy and Microanalysis, 2015, 21, 325-326.	0.4	2
52	Revealing Near-Surface to Interior Redox upon Lithiation in Conversion Electrode Materials Using Electron Microscopy. Microscopy and Microanalysis, 2015, 21, 1369-1370.	0.4	0
53	Shape-Controlled Narrow-Gap SnTe Nanostructures: From Nanocubes to Nanorods and Nanowires. Journal of the American Chemical Society, 2015, 137, 15074-15077.	13.7	42
54	Transitions from Near-Surface to Interior Redox upon Lithiation in Conversion Electrode Materials. Nano Letters, 2015, 15, 1437-1444.	9.1	97

ΚΑΙ ΗΕ

#	Article	IF	CITATIONS
55	Sodiation Kinetics of Metal Oxide Conversion Electrodes: A Comparative Study with Lithiation. Nano Letters, 2015, 15, 5755-5763.	9.1	122
56	Gallium Sulfide–Singleâ€Walled Carbon Nanotube Composites: Highâ€Performance Anodes for Lithiumâ€lon Batteries. Advanced Functional Materials, 2014, 24, 5435-5442.	14.9	102
57	Hydrothermal synthesis, magnetic and electromagnetic properties of hexagonal Fe3O4 microplates. Journal of Magnetism and Magnetic Materials, 2014, 361, 161-165.	2.3	18
58	A facile route to monodisperse MPd (M = Co or Cu) alloy nanoparticles and their catalysis for electrooxidation of formic acid. Nanoscale, 2014, 6, 6970-6973.	5.6	92
59	Structural and Magnetic Evolution of Bimetallic MnAu Clusters Driven by Asymmetric Atomic Migration. Nano Letters, 2014, 14, 1362-1368.	9.1	20
60	Sodiation <i>via</i> Heterogeneous Disproportionation in FeF ₂ Electrodes for Sodium-Ion Batteries. ACS Nano, 2014, 8, 7251-7259.	14.6	89
61	Nanocatalyst Superior to Pt for Oxygen Reduction Reactions: The Case of Core/Shell Ag(Au)/CuPd Nanoparticles. Journal of the American Chemical Society, 2014, 136, 15026-15033.	13.7	172
62	Expanded graphite as superior anode for sodium-ion batteries. Nature Communications, 2014, 5, 4033.	12.8	1,472
63	A New Design for Measuring Potentials in Operando Nanoelectronic Devices by Electron Holography. Microscopy and Microanalysis, 2014, 20, 266-267.	0.4	0
64	Probing the Local Chemical and Structural Ordering of Iron Oxyfluoride. Microscopy and Microanalysis, 2014, 20, 430-431.	0.4	0
65	Discovering a Novel Sodiation in FeF2 Electrodes for Sodium-Ion Batteries. Microscopy and Microanalysis, 2014, 20, 490-491.	0.4	1
66	Diagnosing Nanoelectronic Components Using Coherent Electrons. Nano Letters, 2013, 13, 4815-4819.	9.1	5
67	Silicon nanowires: electron holography studies of doped p–n junctions and biased Schottky barriers. Nanotechnology, 2013, 24, 115703.	2.6	27
68	Mapping magnetic fields of Fe3O4 nanosphere assemblies by electron holography. Journal of Applied Physics, 2013, 113, .	2.5	19
69	Distinguishing P-N Junction and Schottky Barrier in a Working Silicon Nanowire Diode. Microscopy and Microanalysis, 2013, 19, 1356-1357.	0.4	0
70	Theoretical and Experimental Characterization of Structures of MnAu Nanoclusters in the Size Range of 1–3 nm. ACS Nano, 2011, 5, 9966-9976.	14.6	16
71	Direct Observation of Magnetic Domain Wall Propagation in NiFe Nanowires. Microscopy and Microanalysis, 2010, 16, 574-575.	0.4	0
72	Synthesis and Characterization of Crystalline Silicon Carbide Nanoribbons. Nanoscale Research Letters, 2010, 5, 1264-1271.	5.7	99

Kai He

#	Article	IF	CITATIONS
73	Quantitative phase imaging of nanoscale electrostatic and magnetic fields using off-axis electron holography. Ultramicroscopy, 2010, 110, 375-382.	1.9	45
74	Effects of vortex chirality and shape anisotropy on magnetization reversal of Co nanorings (invited). Journal of Applied Physics, 2010, 107, .	2.5	26
75	Remanent states and magnetization reversal of nanopatterned spin-valve elements using off-axis electron holography. Journal of Applied Physics, 2009, 105, 07D517.	2.5	4
76	Vortex Formation During Magnetization Reversal of Co Slotted Nanorings. IEEE Transactions on Magnetics, 2009, 45, 3885-3888.	2.1	4
77	Observation of asymmetrical pinning of domain walls in notched Permalloy nanowires using electron holography. Applied Physics Letters, 2009, 95, 182507.	3.3	18
78	Direct visualization of three-step magnetization reversal of nanopatterned spin-valve elements using off-axis electron holography. Applied Physics Letters, 2009, 94, .	3.3	15
79	Synthesis and characterization of single-crystalline MnFe2O4 nanorods via a surfactant-free hydrothermal route. Journal of Magnetism and Magnetic Materials, 2008, 320, 2672-2675.	2.3	104
80	A facile molten salt route to K2Nb8O21 nanoribbons. Ceramics International, 2008, 34, 435-437.	4.8	21
81	Fractal growth of single-crystal α-Fe2O3: From dendritic micro-pines to hexagonal micro-snowflakes. Materials Letters, 2008, 62, 739-742.	2.6	44
82	Hydrothermal synthesis and characterization of single-crystalline Fe3O4 nanowires with high aspect ratio and uniformity. Materials Letters, 2007, 61, 3159-3162.	2.6	67